Astron. Astrophys. 358, 535–546 (2000)

ASTRONOMY AND ASTROPHYSICS

Self-enrichment in ω Centauri

C. Ikuta and N. Arimoto

Institute of Astronomy, School of Science, University of Tokyo, Mitaka, Tokyo 181-8588, Japan

Received 2 July 1999 / Accepted 19 November 1999

Abstract. The origin of abundance spreads observed in ω Centauri is studied in the context of the self-enrichment scenario. Five chemical evolution models are constructed and are compared with empirical metallicity distribution of ω Cen. After a series of simulations, it is found that neither of closed-box, outflow, nor infall models can reproduce the empirical metallicity distribution of ω Cen, while a modified outflow model with a bimodal initial mass function (IMF) gives a metallicity distribution that fits closely to the empirical ones. In the modified outflow model, long-lived stars are assumed to form after the first explosion of type II supernovae (SNII) in a proto-cloud. The modified outflow model involves gas infall at the very first chemical evolution. Thus we conclude that self-enrichment causes the abundance dispersion in ω Cen. A success of the outflow model with the bimodal IMF implies that low mass stars in a globular cluster (GC) should have formed in the gas already enriched by the first generation of SNII.

This scenario, originally proposed by Cayrel (1986), can explain a lack of globular clusters with [Fe/H]$\lesssim -2.2$ in the Milky Way Galaxy.

Key words: Galaxy: globular clusters: general – Galaxy: globular clusters: individual: ω Centauri – stars: abundances – stars: Population II – galaxies: abundances – galaxies: evolution

1. Introduction

The first comprehensive study of a peculiar globular cluster ω Centauri, including photographic photometry and proper motion analysis for several thousands stars, was undertaken by Woolley (1966). The resulting colour-magnitude diagram was discussed by Dickens & Woolley (1967), who showed a large colour width of the red giant branch (RGB) stars of ω Cen. Cannon & Stobie (1973) confirmed later the spread of RGB colours and argued that it must result from a heavy element abundance dispersion. Freeman & Rodgers (1975) revealed a diversity of the composition of observed RR Lyrae variables and suggested that it may come from metal enrichment of the gas during proto-cloud collapse. Butler et al. (1978) observed nearly half of the cluster RR Lyrae variables and found an intrinsic range in [Fe/H] from -2.0 to -1.1.

However, the origin of abundance scatter observed in ω Cen is still an open question. Abundance anomalies of C, N, O, Na, Mg, and Al are often observed in Galactic globular clusters (GCs), and are interpreted as being a mixing effect at the later stage of stellar evolution (e.g., Kraft 1994). Unlike other GCs, ω Cen and probably also M22 (Lehnert, Bell, & Cohen 1991) show the abundance spreads of the iron-peak elements. Since no stellar evolution theory predicts changes in the abundances of these elements, this is one of the interesting features of the cluster. Omega Cen is the brightest (Harris & Racine 1979), potentially the most massive, and the dynamically youngest cluster (Trager et al. 1995) in the Milky Way Galaxy. Omega Cen is also one of the most flattened clusters (e.g. Freeman & Norris 1981). Meylan & Mayor (1986) suggested that the flattening results from rotation, because the rotational velocity tightly correlates with the ellipticity. Since ω Cen has lots of peculiarities and locates relatively close to the solar system (~ 5.2 kpc; Meylan 1987), photometric and spectroscopic observations have been carried out intensively. Despite these efforts, the process of chemical enrichment and the causes of abundance spreads are not yet well understood. Kraft (1979) suggested four possible explanations, and Smith (1987) discussed them again in his review paper: (i) the proto-cloud of ω Cen already had abundance inhomogeneity; (ii) stars in ω Cen were enriched when it passed by a Galactic disc; (iii) ω Cen was formed via a merger of less massive GCs; (iv) ω Cen was self-enriched.

In this paper, focusing on the abundance scatters of elements, we investigate whether a self-enrichment scenario can explain observations of the chemical properties. We also cannot completely dismiss the first scenario. However, it is rather *ad hoc* to postulate a primordial cloud abundance inhomogeneity and it is still necessary to explain how the abundance dispersions were brought into a proto-cloud and why this phenomenon is conspicuous in ω Cen but not in other GCs. True, dust segregation may partly explain the abundance spreads in the proto-cloud. Bhatt (1988) suggested that the abundance scatter should be enhanced by the dust segregation, since the dust collecting heavy elements fell into the proto-cloud centre by gravitational and viscous forces, and consequently the inner region attains higher

Send offprint requests to: C. Ikuta

metallicity than the outer. Eq. (7) of Bhatt (1988) gives 0.1 Gyr as a time required to grow a metallicity difference up to ~ 1 dex. On the other hand, stars of the first generation in the proto-cloud should be formed in a free-fall time scale, typically ~ 0.01 Gyr (e.g., Cayrel 1986). Lifetimes of massive stars are around a few Myr. This means that dust grains were disintegrated by UV radiation from newly formed stars before the abundance difference reaches to ~ 1 dex. Thus, the dust segregation hypothesis alone cannot explain the abundance scatters of ω Cen.

The accretion scenario is not plausible either. Most GCs show little evidence for the scatter (Kraft 1979). This is also true for GCs which are on the orbit that closely passes by the Galactic disc (e.g. Dauphole et al. 1996), despite this they are most likely to be contaminated. Observed [α/Fe] ratios are over-abundant (Norris & Da Costa 1995), which implies that stars in ω Cen were not enriched by type Ia supernovae (SNIa) which synthesise a large amount of iron-peak elements. If stars in ω Cen were contaminated by the disc gas, [α/Fe] should be close to solar, since the disc gas has nearly solar composition (Edvardsson et al. 1993). Thus, we put aside the second possibility.

Third, the merging formation scenario is not applicable. Norris et al. (1997) favoured this scenario because, (i) the metallicity distribution (MD; Norris et al. 1996, hereafter NFM96) is bimodal; (ii) N-body simulations by Makino et al. (1991) predicted that merging of GCs result in a flattened system, and more significantly (iii) the metal-rich ([Ca/H] > -1.2) giants radially concentrate at the inner region than the metal-poor ([Ca/H] ≤ -1.2) ones and rotate differently. First, the bimodal MD claimed by NFM96 was not confirmed by Suntzeff & Kraft (1996; hereafter SK96) who derived the MDs for giants and subgiants, individually. If the merger creates a bimodal MD, the metallicity dispersions must already have been in both pre-merging clusters. Searle (1977) predicted that a merged cluster should have a bimodal MD. In his model, all the GCs have metallicity dispersions. Thus, Searle's model is not applicable for the Galactic GCs. Second, the N-body simulation performed by Makino et al. (1991) is for a binary GC. On the other hand, no binary GC has been discovered in the Milky Way Galaxy yet. It seems to be difficult for GCs to encounter randomly and to become a single system (Icke & Alcaíno 1988) because orbital velocities ($v \geq 200$ km s^{-1}; Dauphole et al. 1996) of observed GCs are much larger than their internal velocity dispersions ($\sigma \sim 10$km s^{-1}; Cudworth 1976). Third, the observed number of metal-rich stars is small and is affected by a sampling bias (NFM96; SK96). Thus it is not conclusive that the metal-rich and the metal-poor stars have different positional and dynamical properties.

Therefore, we suppose that the self-enrichment causes the abundance anomalies in ω Cen. Cayrel (1986) investigated the reason why no population III GCs have been discovered yet and found that it is due to an enrichment by the first stars born in a cloud with the primordial abundance. Simulating the evolution of supernova remnants in a cloud, Morgan & Lake (1989) concluded that every GC can be enriched at least by one SNII. Since ω Cen is a massive GC ($\sim 3\,10^6 M_\odot$; Meylan & Mayor 1986), it is likely that the enriched gas can be recycled and the metallicity scatters are produced. Based on accurate Strömgren photometry of ω Cen, Hughes & Wallerstein (1998) have recently shown that the most meta-poor stars are 14 Gyr old, the intermediate metallicity ones are 12 Gyr old and the most metal-rich ones are 10 Gyr old. This might give direct proof that ω Cen has produced stars of increasing metallicity over a span of about 4 Gyrs, although the resulting age span of course depends on stellar evolutionary tracks adopted. Recently, NFM96 and SK96 obtained the metallicity distribution functions (MDF) of ω Cen. These studies show that the empirical MDF has a long tail extended toward higher metallicity and that an analytical MDF predicted by a simple model of chemical evolution fails to explain the observed MDF (NFM96; SK96).

In this paper, we show that an outflow model can explain the observed MDF. We construct three models; outflow, infall, and modified outflow models. In the first two models, we assume that the mass range of newly formed stars is from $0.1 M_\odot$ to $60 M_\odot$ and time invariant. In the third model, which is the modified outflow model, the lower limit of newly formed stars s assumed to change after the first SNII explosions. Thus the IMF is not time invariant any more. The idea comes from Cayrel (1986). We find that the modified outflow model with the bimodal IMF provides the metallicity distribution which gives an acceptable match to the data. If the numerical MDF should be more strictly compared with the observed one, in addition to the bimodal IMF and the outflow, the gas infall is necessary at the very early stage of chemical evolution.

The outline of the paper is as follows. In Sect. 2, we review the observed MDF. In Sect. 3, the model prescriptions are given and the results are confronted with the observations, and in Sect. 4, a chemical enrichment in GCs is discussed. We also discuss briefly spatial metallicity distribution and metallicity gradients observed in elliptical galaxies in Sect. 4. Our conclusions are summarised in Sect. 5.

2. The observed metallicity distribution

For elements such as Fe and Ca, long-lived stars should keep the original abundances of the interstellar medium from which they formed. The mixing in stellar interior, such as convection and meridional circulation, should have no effect on these elements, although light elements such as C, N, and O are likely to change considerably. Therefore, the metallicity distribution is expected to provide information on chemical enrichment history and is considered as a powerful clue to trace the chemical evolution in ω Cen. In this section, we compare the MDF derived by NFM96 and by SK96 and review the properties.

SK96 measured stellar metallicities of bright giant stars ($12.2 < \mathrm{V} < 12.8$; hereafter BG sample) and fainter subgiant stars ($14.8 < \mathrm{V} < 15.3$; hereafter SG sample) using the near-infrared Ca II triplet lines at $\lambda\lambda 8542 - 8662$ Å and presented the [Fe/H] - MDF of each sample in the iron abundance scale. On the other hand, NFM96 measured [Ca/H] based on the near-infrared Ca II triplet and the Ca II H and K lines and presented the [Ca/H] - MDF. Since both authors measured equivalent widths W(Ca) of the Ca lines and reduced equivalent widths W'(Ca)

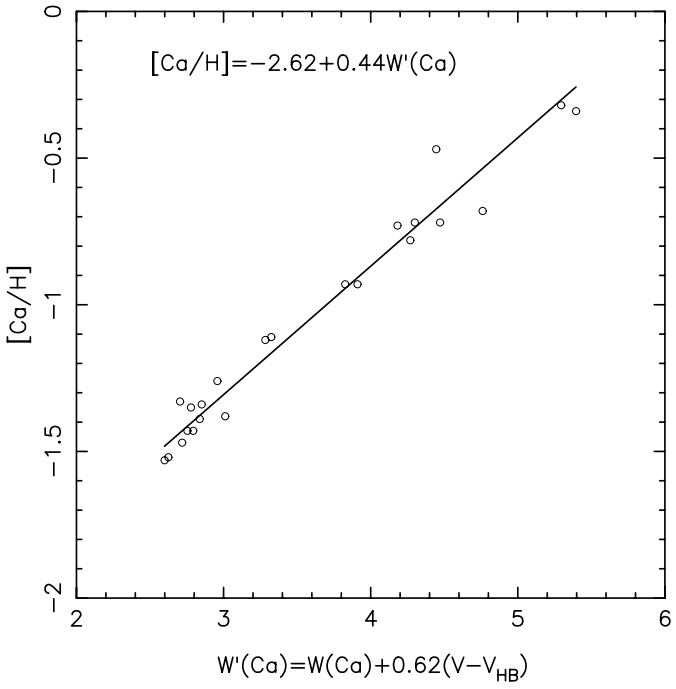

Fig. 1. Calibration of [Ca/H] as a function of the reduced calcium equivalent width W'(Ca) of the BG sample by SK96 in units of Å. The abundance data by high dispersion spectroscopy were taken from Norris & Da Costa (1995)

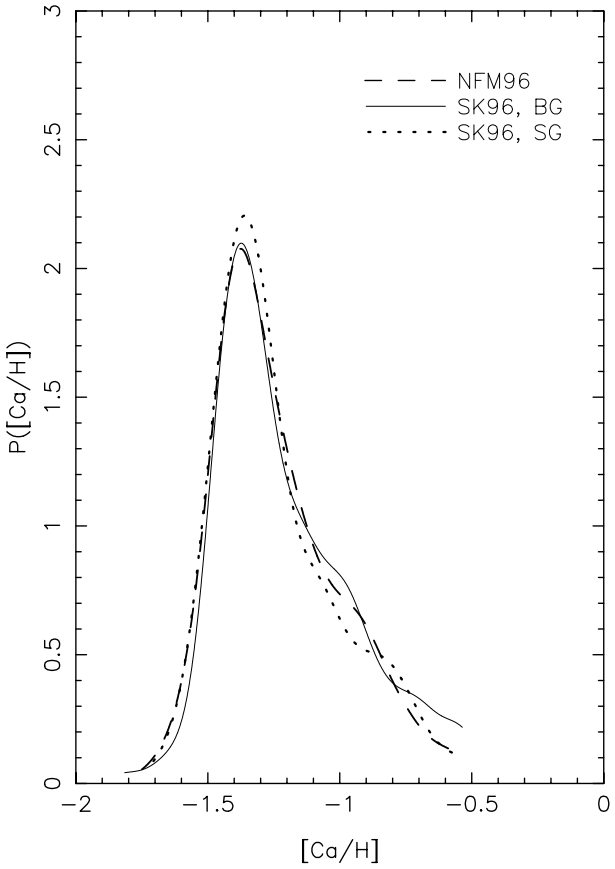

Fig. 2. Observed metallicity distribution functions of [Ca/H]. Dashed line represents the sample observed by NFM96. Solid and dotted lines give the BG and the SG samples (SK96), respectively

which correlate with [Ca/H] better than [Fe/H] (see Fig. 7 in SK96), we adopt [Ca/H] as a common scale.

Fig. 1 gives a correlation between W'(Ca) and [Ca/H] for the BG sample, where W'(Ca) is given as a function of $(V - V_{\rm HB})$, which is a difference between the observed V magnitude of a star and that of the horizontal branch (HB) of a cluster (SK96):

$$\mathrm{W}'(\mathrm{Ca}) = \mathrm{W}(\mathrm{Ca}) + 0.62(V - V_{\rm HB}). \quad (1)$$

In Fig. 1, [Ca/H] is taken from Norris & Da Costa (1995) who observed 40 stars in ω Cen with high-dispersion spectroscopy. We derive the following formula for $-1.5 \leq [\mathrm{Ca/H}] \leq -0.3$ by a least-square fitting:

$$[\mathrm{Ca/H}] = -2.62 + 0.44\mathrm{W}'(\mathrm{Ca}). \quad (2)$$

For stars out of this range, we extrapolate Eq. (2). We do not consider that this dramatically changes the metallicity distribution at [Ca/H] < -1.5, since the number of such metal-poor stars is small, as we see below. The frequency distribution of [Ca/H] at [Ca/H]> -0.5 will be discussed in detail later. The following equation (SK96) is used for the SG sample instead of Eq. (1):

$$\mathrm{W}'(\mathrm{Ca}) = \mathrm{W}(\mathrm{Ca}) + 0.35(V - V_{\rm HB}) - 0.19, \quad (3)$$

and calculate [Ca/H] by using Eq. (2).

Fig. 2 shows the three MDFs, where the dashed line represents the sample taken from NFM96, while the solid and the dotted lines represent the BG and the SG samples of SK96, respectively. Usually an observed MDF is presented in the form of a histogram. However, we prefer to use a continuous distribution function to avoid artificial distortion by a binning and to take into account observational uncertainties properly (Searle & Zinn 1978; Laird et al. 1988). The definition of such a continuous MDF $P(z)$ is given by Laird et al. (1988):

$$P(z) = \frac{1}{N\sigma\sqrt{2\pi}} \sum_{i=1}^{N} \exp\left(-\frac{(z - z_i)^2}{2\sigma^2}\right), \quad (4)$$

where σ gives a typical error in the observed values $z_1, z_2, ..., z_N$ and is adopted $\sigma = 0.05$ for the data by NFM96 and $\sigma = 0.07$ for these by SK96, respectively.

In Fig. 2, we present the MDF for [Ca/H]< -0.5 following NFM96, because sampling bias is significant at the higher abundance, a more detailed discussion is given in SK96. By observing a magnitude limited sample, data is suspected to be biased and metal-rich stars might be under-represented, because a fraction of stars brighter than a given magnitude is a function of abundance. In Eqs. (1) and (2), we assume that stars of the BG sample and those taken from NFM96 lie on the RGB rather than on the asymptotic giant branch (AGB). Although the abundance distribution of AGB stars may differ from that of the RGB stars because of dependence of post-RGB evolution on mass and abundance, inclusion of the AGB stars will not seriously distort the observed MDF (NFM96). Thus, it seems reasonable to

consider that the MDF in Fig. 2 represents the global MDF of ω Cen.

The MDFs of SK96 and NFM96 samples are almost identical. Both rise sharply at [Ca/H]$\simeq -1.7$ and reach a well-defined peak at [Ca/H]$\simeq -1.4$, and then gradually decline. The MDF is characterised by a tail extended to higher abundance which contains more stars than a prediction of a simple chemical evolution model (NFM96; SK96). There is a small bump at [Ca/H]$\simeq -0.9$ in the NFM96 sample, at [Ca/H]$\simeq -1$ and [Ca/H]$\simeq -0.6$ in the BG and the SG samples of SK96, respectively. We do not regard these bumps as significant, because of the under-sampling effect mentioned before. NFM96 inferred that the stars with [Ca/H]$\simeq -0.7$ are under-sampled by some 40% with respect to those having [Ca/H]$\simeq -1.7$.

One might consider these second peaks as an effect of SNIa which produce not only the iron-peak elements but also calcium (Nomoto et al. 1984). However, [α/Fe] of stars in ω Cen is super-solar (Norris & Da Costa 1995), which means that the stars in ω Cen were formed in clouds which were not enriched by SNIa. In other words, duration of star formation must be shorter than a typical lifetime ($\sim 1-2$ Gyr) of SNIa progenitors, and thus these bumps should not be related to SNIa.

We regard the well-defined peak, the sharp distribution, and the metal-rich tail as the key features of the empirical MDF of ω Cen. A degree of the asymmetry of a distribution function can be described by a statistical value, skewness. A positive value of skewness signifies a distribution with an asymmetric tail extending out toward larger measured value, while a negative value signifies a distribution whose tail extends out toward smaller value. The definitions and more detailed descriptions are given in Ikuta & Arimoto (1999). The skewness for the observed MDF of NFM96 is 0.73, which tells again that the MDF has a large asymmetric tail to the higher abundance. We will use the skewness to constrain chemical evolution models.

3. Theoretical metallicity distribution

3.1. Closed box and outflow models

A chemical evolution model traces the abundance changes in the interstellar matter (ISM) of a region, from which the stellar abundance distributions are derived. A detailed derivation of the fundamental equations can be found in Tinsley (1980). We assume well-mixing of the interstellar matter and relax the instantaneous recycling approximation throughout this paper. In this subsection, we study a closed-box model and an outflow model following Hills (1980) who pointed out that the GCs are slowly mass-losing systems.

Generally stellar birth rate is separated into two independent functions. The birth rate of stars with mass between m and $m+dm$ is described as $C(t)\phi(m)dm$, where $C(t)$ and $\phi(m)$ are the star formation rate (SFR) and the IMF, respectively. In this model, the IMF is assumed to be a time invariant function with a power-law spectrum. Normalising to unity, we have

$$\phi(m) = \frac{(x-1)m_l^{x-1}}{1-(m_l/m_u)^{x-1}} m^{-x}, \tag{5}$$

where the lower and the upper mass limits are $m_l = 0.1M_\odot$ and $m_u = 60M_\odot$, respectively. The Salpeter IMF has $x = 1.35$ in this definition. The SFR is assumed to be proportional to the gas fraction $f_{\rm g}(t)$:

$$C(t) = \frac{M_{\rm T}}{\tau_{\rm sf}} f_{\rm g}(t) = \frac{M_{\rm g}(t)}{\tau_{\rm sf}}, \tag{6}$$

with

$$f_{\rm g}(t) \equiv M_{\rm g}(t)/M_{\rm T}, \tag{7}$$

where $\tau_{\rm sf}$ and $M_{\rm T}$ are the time scale of star formation and the initial total mass of ω Cen, respectively. The gas mass $M_{\rm g}(t)$ changes through star formation and gas outflow:

$$\frac{dM_{\rm g}(t)}{dt} = -C(t) + E(t) - B(t), \tag{8}$$

where $E(t)$ is the gas ejection rate from dying stars. $B(t)$ is the gas outflow rate (OFR) and is assumed to be given by $M_{\rm g}(t)$ and the outflow time scale $\tau_{\rm of}$,

$$B(t) = \frac{M_{\rm T}}{\tau_{\rm of}} f_{\rm g}(t) = \frac{M_{\rm g}(t)}{\tau_{\rm of}}. \tag{9}$$

The equation governing the evolution of the abundance of i-th element $Z_i(t)$ is given by:

$$\frac{d(Z_i M_{\rm g})}{dt} = -Z_i C(t) + E_{Z_i}(t) + Z_i(0) M_{\rm T}, \tag{10}$$

where $E_{Z_i}(t)$ is the total ejection rate of processed and unprocessed i-th element and $Z_i(0)$ is the initial abundance of i-th element in a proto-cloud. We calculate $E(t)$ and $E_{Z_i}(t)$ from the following integrals:

$$E(t) = \int_{m_t}^{m_u} (1-w_m) C(t-t_m)\phi(m) dm, \tag{11}$$

$$E_{Z_i}(t) = \int_{m_t}^{m_u} [(1-w_m) Z_i(t-t_m) + p_{im} C(t-t_m)\phi(m)] dm, \tag{12}$$

where t_m is the lifetime of a star with mass m. The lower limit m_t is the stellar mass with lifetime $t_m = t$. Nucleosynthesis data w_m and p_{im} are the remnant mass fraction and the mass fraction of processed and unprocessed i-th element, both are taken from Thielemann, Nomoto, & Hashimoto (1996). Although stellar metallicity could affect both w_m and p_{im}, this is still debated. Thus we ignore these possible effects and adopt the values calculated for the solar abundance. We assume that the lower mass limit $m_{l,\rm II}$ for a progenitor of SNII is $10M_\odot$ (Tsujimoto et al. 1995).

There are two different points of view to explain the initial metallicity of GCs: (1) a proto-cloud is enriched by itself, (2) a proto-cloud is formed from previously enriched gas. Following Lee et al. (1995), we assume that a proto-cloud of ω Cen was enriched and initially had a homogeneous composition. Hence, the initial metallicity $Z_i(0)$ of the proto-cloud is treated as a parameter.

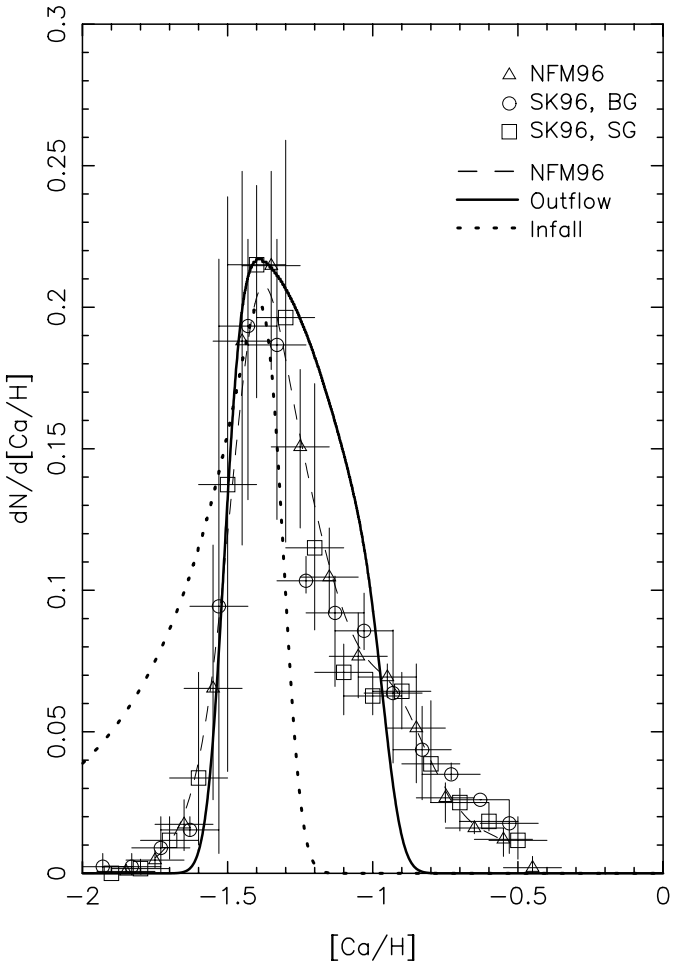

Fig. 3. A comparison of the empirical and the theoretical MDFs. The solid line represents the best fit MDF of the outflow model described in Sect. 3.1, and the dotted line gives that of the infall model in Sect. 3.2. The dashed line illustrates the empirical MDF obtained by NFM96's data. Symbols indicate each sample as following: (*triangles*) NFM96; (*circles*) the BG of SK96; (*squares*) the SG of SK96. The vertical axis gives a number normalised by the sum of each sample

Aiming to find a good model prescription, we simulated ~ 60000 models, since the parameters of chemical evolution such as $\tau_{\rm SF}$, $\tau_{\rm OF}$, x, and duration of star formation T are unknown. Fitting goodness is evaluated by a χ^2-test with five degrees of freedom. Model grids are the following:

$$\begin{aligned}
\tau_{\rm sf} &= 0.001,\ 10^{-2.0+0.3i}\ (i=0,...,10), 3,\ 5\ \ {\rm Gyr},\\
\tau_{\rm of} &= 0,\ 0.001,\ \left[10^{-2.0+0.3i}\ (i=0,...,10)\right], 3,\ 5\ \ {\rm Gyr},\\
x &= 0.7+0.2i\ (i=1,...,7),\\
T &= 10^{-2.0+i\Delta T}\ (i=0,...,29)\ \ {\rm Gyr},\\
{\rm [Ca/H]}_0 &= -\infty, -1.6, -1.5, -1.4,
\end{aligned} \tag{13}$$

where $\Delta T = 7.25\cdot 10^{-2}$ Gyr, $[{\rm Ca/H}]_0$ is the initial calcium abundance, and $\tau_{\rm of}=0$ corresponds to a closed-box model.

In Fig. 3, the solid line represents a model which gives the smallest $\chi^2=16.2$, and the dashed line represents the empirical MDF by NFM96. The model has $\tau_{\rm sf}=0.68$ Gyr, $\tau_{\rm of}=1$ Gyr, $x=1.9$, and $[{\rm Ca/H}]_0=-1.5$. The best fit MDF is realized at $T=1.27$ Gyr. In despite of the good χ^2 value, it is obvious from eye judgement that the theoretical MDF is inconsistent with the observations. There are fewer stars of $[{\rm Ca/H}]<-1.6$ and $[{\rm Ca/H}]>-0.8$, while more stars of $-1.3<[{\rm Ca/H}]<-1$. The observations show that the lowest stellar metallicity in ω Cen is around $[{\rm Ca/H}]\simeq -1.7$. This might imply that the mother cloud of long-lived stars in ω Cen had already this metallicity. However, too many stars with the initial abundance are formed when we assume $[{\rm Ca/H}]_0=-1.7$ and such models are also inconsistent with the observations. This resembles the G-dwarf problem in the solar neighbourhood.

Although the theoretical MDF has a tail slightly extended to the higher abundance, it is not long enough compared with the empirical ones. The skewness quantitatively describes this. The skewness for the theoretical MDF (0.73) is equal to 0.31, which is smaller than that of the empirical MDF by at least a factor of two. We find that a good model cannot be selected based only on the χ^2-test, since it is only an integrated difference between a numerical and the observed MDF. Therefore, we use the two statistics to determine good model prescriptions. A global fitting goodness is quantified by the χ^2-test, while similarity of shape of the empirical and theoretical MDFs is measured by the skewness.

3.2. Infall model

To avoid the so-called G-dwarf problem, we consider an infall model which is known to solve the G-dwarf problem in the solar neighbourhood (Tinsley 1980).

Instead of Eq. (8), the evolution of the gas mass is given by

$$\frac{dM_{\rm g}(t)}{dt} = -C(t)+E(t)+A(t), \tag{14}$$

where $A(t)$ is a gas infall rate and is assumed to be an exponentially decreasing function:

$$A(t) = \frac{M_{\rm T}}{\tau_{\rm in}} e^{-t/\tau_{\rm in}}, \tag{15}$$

where $\tau_{\rm in}$ is an infall time scale. The abundance evolution of i-th element is described as

$$\frac{d(Z_i M_{\rm g})}{dt} = -Z_i C(t) + E_{Z_i}(t) + Z_i' A(t), \tag{16}$$

where Z_i' is an abundance of i-th element in the infalling gas. Other model prescriptions are the same as those of the outflow model. We perform more than 60000 simulations. The model grids are the same as before except for $\tau_{\rm in}$. We adopt $\tau_{\rm in}=0.001,\ \left[10^{-2.0+0.3i}\ (i=0,...,10)\right],\ 3,\ 5$ Gyr instead of a sequence of $\tau_{\rm of}$, where we select a model by the χ^2-test with five degrees of freedom.

In Fig. 3, the dotted line represents the MDF of the best fit infall model ($\chi^2=62$), whose $\tau_{\rm sf}$, $\tau_{\rm in}$, T, and x are 0.25 Gyr, 0.25 Gyr, 0.034 Gyr and 1.1, respectively. This model initially had the primordial abundance. We notice that the MDF of the infall model has a tail extended to the lower abundance and

obviously fails to fit the observed MDF. Calculating models assuming $(\mathrm{Ca/H})_0 = 0$ and/or a high infall rate, we test and find that a tail of each MDF resulting from the infall model always extends to the lower metallicity too much. In conclusion, no good prescription is found in the outflow (including the closed-box) and the infall models.

3.3. Models with a bimodal IMF

The fitting goodness of the MDFs discussed in Sects. 3.1 and 3.2 suggests that the outflow model is more or less favoured. The essential problem of this model is that too many stars with the initial abundance were formed. In the previous models, we have assumed that the low and the high mass stars were born simultaneously. This assumption might be an over simplification when we study the first generation of stars in GCs.

Here, we consider another model proposed by Cayrel (1986) who investigated the reason why no metal-free GCs have been observed. He predicted that all GCs were self-enriched. His basic argument is that the time scales of formation (~ 0.01 Gyr) and evolution (~ 0.001 Gyr) of massive stars are shorter than the corresponding time scale for low-mass stars. In the free-fall collapse, the density will be largest at the centre of a cloud, where the first stars form. The central stars are likely to be massive because of a shorter time scale of fragmentation than that of low mass stars. The first SNII explosions occur at the central core toward which the gas is infalling. The bulk of star formation with a full spectrum range of stellar masses will occur in the shock between the collapsing envelope and the SNII-driven wind. In this view, low mass stars are expected to form in the gas enriched by the first SNII explosions. This scenario can naturally explain the observed lower metal cutoff ([Fe/H]$\simeq -2.2$) of GC systems in the Milky Way Galaxy.

Morgan & Lake (1989) investigated a possibility of self-enrichment in a GC. By simulating the evolution of supernovae remnants in a proto-cloud, they examined whether the remnants can cool down and become gravitationally bound. They found that every GC should survive at least one supernova explosion and can be enriched. Thus we construct a model based on the scenario proposed by Cayrel (1986).

3.3.1. Bimodal IMF

To take into account the delayed formation of low-mass stars suggested by Cayrel (1986), we assume that the lower mass limit m_l of the IMF is equal to $m_{l,\mathrm{II}}$ until the onset of the first SNII explosion; that is, star formation with a full mass spectrum occurs only after the first SNII supernova explosion. Eq. (5) is replaced by

$$\phi(m) = \frac{(x-1)m_{l,\mathrm{II}}^{x-1}}{1-(m_{l,\mathrm{II}}/m_u)^{x-1}} m^{-x} \quad (m_{l,\mathrm{II}} < m < m_u), \quad (17)$$

for $(t < t_{u,\mathrm{II}})$ and

$$\phi(m) = \frac{(x-1)m_l^{x-1}}{1-(m_l/m_u)^{x-1}} m^{-x} \quad (m_l < m < m_u), \quad (18)$$

for $(t \geq t_{u,\mathrm{II}})$, where $t_{u,\mathrm{II}}$ is the lifetime of the most massive SNII progenitor and is assumed to be equal to that of stars with m_u. Since the total amount of metals which are ejected by the first SNII is unknown, metallicity $[\mathrm{Ca/H}]_0$ locked in the first generation of long-lived stars is taken as a parameter. Other model parameters are the same as those described in Sect. 3.1. More than 60000 models are simulated and model grids are the same as those of the outflow model. As a result, we find two models (models A1 and A2) which give good χ^2 with six degrees of freedom and skewness. Their χ^2 values, skewness, and parameters are given in Table 1.

Models A1 and A2 have been selected ignoring whether the gas can be bound against energy injection from SNII. When the cumulative thermal energy $E_{\mathrm{th}}(t)$ from SNII exceeds the gas binding energy $\Omega_{\mathrm{g}}(t)$, the gas should be expelled rapidly and hence the star formation must be terminated (Arimoto & Yoshii 1987). If the epoch (T_{w}) of $E_{\mathrm{th}}(t) = \Omega_{\mathrm{g}}(t)$ comes before a theoretical metallicity dispersion grows to ~ 1 dex, the results of models A1 and A2 are unphysical. Another possible case of gas ejection from a system is that the entire volume of the system covered with supernovae remnants (SNRs) is expanding faster than the escape velocity at the centre of the system (Ikeuchi, 1977). This condition is not satisfied prior to the former one in any case, since a SNR is rapidly cooled down due to high density of the surrounding interstellar medium and can fill only a small area (typically several pc in radius). Thus we only discuss the evolution of $E_{\mathrm{th}}(t)$ and $\Omega_{\mathrm{g}}(t)$.

The rotation curve of ω Cen presented by Meylan & Mayor (1986) implies that the dark matter distributes similarly to luminous matter and that ω Cen does not have a massive diffused dark halo. Therefore, the following equation (Saito 1979) is suitable to describe $\Omega_{\mathrm{g}}(t)$:

$$\Omega_{\mathrm{g}}(t) = \Omega_{\mathrm{T}} f_{\mathrm{g}}(t)\,(2 - f_{\mathrm{g}}(t))\,, \quad (19)$$

where Ω_{T} is the total binding energy. From analysing surface brightness distributions and line-of-sight velocity dispersions, Saito (1979) derived an empirical relation between Ω_{T} and M_{T} for spheroidals ranging from GCs to elliptical galaxies:

$$\Omega_{\mathrm{T}} = 3.31\,10^{51} \left[\frac{M_{\mathrm{T}}}{10^6 M_\odot}\right]^{1.45} \ \mathrm{erg}. \quad (20)$$

Although Eq. (20) is based upon the present-day properties of spheroidals, we assume that we can trace back the dynamical state from information available today. Using Eq. (20), the radius R of a viriarized spherical system is given as

$$R = 13.1 \left[\frac{M_{\mathrm{T}}}{10^6\ M_\odot}\right]^{0.55} \ \mathrm{pc}. \quad (21)$$

The virial theorem says that a system with no kinetic energy initially attains virial equilibrium by reducing a radius to half of the initial value. Assuming that the initial radius is equal to $2R$ and that the matter in the system distributes homogeneously, we can calculate the average density $\rho(t)$:

$$\rho(t) \ = \ \frac{3M_{\mathrm{g}}(t)}{4\pi(2R)^3}$$

Table 1. Parameters of models A1, A2, B, and C described in Sect. 3.3. Column (1): model identification, Column (2): fitting goodness, Column (3): initial calcium abundance, Column (4): IMF power, Column (5): time scale of star formation in Gyr, Column (6): time scale of outflow, Column (7): time scale of inflow, Column (8): duration of star formation, Columns (9) & (10): [Ca/H] and gas fraction at T, Column (11): epoch of $E_{\rm th} = \Omega_{\rm g}$ in Gyr, Column (12): skewness of each model. The skewness of the empirical MDF of NFM96 is 0.73

Model	χ^2	$[\mathrm{Ca/H}]_0$	x	$\tau_{\rm sf}$	$\tau_{\rm of}$	$\tau_{\rm in}$	T	[Ca/H]	$f_{\rm g}$	$T_{\rm W}$	skew
A1	23.2	-1.40	1.3	0.160	0.010	–	0.030	-0.56	0.03	0.030	0.89
A2	25.8	-1.40	1.9	0.025	0.025	–	0.060	-0.53	0.01	0.042	0.95
B	15.8	-1.60	1.9	0.100	0.200	0.030	0.310	-0.79	0.02	0.400	0.38
C	4.5	-1.60	1.9	0.070	0.200	0.070	0.280	-0.65	0.006	0.310	0.58

$$= 7.27\,10^{-21}\left(\frac{M_{\rm g}(t)}{10^6 M_\odot}\right)^{-0.65} \ \mathrm{g\,cm^{-3}} \qquad (22)$$

The cumulative thermal energy $E_{\rm th}(t)$ in the gas is expressed as

$$E_{\rm th}(t) = \begin{cases} 0 & (t < t_{u,\rm II}) \\ \int_{\max(m_t, m_{l,\rm II})}^{m_u} dm & \\ \quad \times \int_0^{t-t_m} \frac{M_{\rm T}}{m}\epsilon(t-t_m-t')C(t')\phi(m)dt & \\ & (t_{u,\rm II} \le t). \end{cases} \qquad (23)$$

The thermal energy content $\epsilon(t)$ inside a SNR is assumed to evolve according to (Cox, 1972),

$$\epsilon(t_{\rm SN}) = \begin{cases} 7.2\,10^{50}\epsilon_0 \ \mathrm{erg} & (0 \le t_{\rm SN} < t_{\rm c}(t)) \\ 2.2\,10^{50}\epsilon_0 (t_{\rm SN}/t_{\rm c}(t))^{-0.62} \ \mathrm{erg} & (t_{\rm c}(t) \le t_{\rm SN}), \end{cases} \qquad (24)$$

where ϵ_0 is an initial blast wave energy in units of 10^{51} erg, $t_{\rm SN}$ is the time elapsed from onset of SNII explosion, and $t_{\rm c}(t)$ is the complete cooling time of the SNR shell:

$$t_{\rm c}(t) = 5.3\,10^{-5}\epsilon_0^{4/17} n(t)^{-9/17} \ \mathrm{Gyr}. \qquad (25)$$

We adopt $\epsilon_0 = 0.75$ (Cox 1972). The surrounding gas density $n(t)$ in $\mathrm{cm^{-3}}$ is assumed to be equal to $\rho(t)/\mu m_{\rm H}$, where $m_{\rm H}$ is the mass of a hydrogen atom and $\rho(t)$ can be obtained from Eq. (22). Neglecting masses of metals, we adopt the mean molecular weight $\mu = 1.3$, since we study a metal-poor object. Hereafter, we adopt $M_{\rm T} = 3\,10^6\,M_\odot$ (Meylan & Mayor 1986). We check and confirm that the subsequent results do not change if we adopt $M_{\rm T} = 5\,10^6\,M_\odot$ (Meylan et al. 1995).

Fig. 4 gives the evolution of $E_{\rm th}/\Omega_{\rm g}$ of models A1 and A2. The epoch ($T_{\rm w}$) of $E_{\rm th}/\Omega_{\rm g} = 1$ is realized at 0.030 and 0.042 Gyr in models A1 and A2, respectively, which are described in Table 1. On the other hand, the resulting durations of star formation of models A1 and A2 are 0.03 and 0.06 Gyr, respectively. Comparing $T_{\rm w}$ with T of each model, we reject model A2. Model A1 satisfies the criterion and the duration of star formation is also consistent with the argument in Sect. 2 that stars in ω Cen should have formed before SNIa explosion.

In Fig. 5, the solid line illustrates the MDF given by model A1, while the dashed one gives the MDF obtained by NFM96. We can say that the modified outflow model of the bimodal IMF can roughly reproduce the observation if we focus on the key features of the empirical MDF such as the well-defined peak and the metal-rich tail. However, discrepancies exist between model A1 and the observations. At [Ca/H]> -1.2, model A1 predicts more stars than the observations. A part of this discrepancy might come from the observational effect of under-sampling as we have mentioned in Sect. 2. We also note that the theoretical MDF is inconsistent with the observations at [Ca/H] < -1.4, and hence, the $\chi^2 (= 23.2)$ is slightly worse than the best fit outflow model in Sect. 3.1.

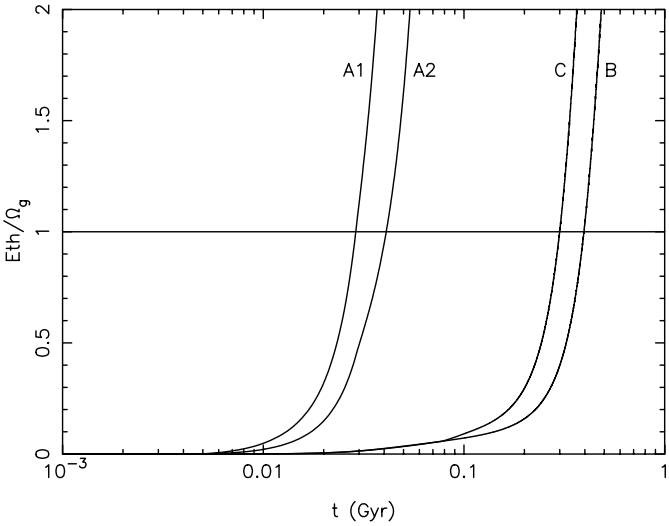

Fig. 4. Evolution of the ratio between the cumulative thermal energy $E_{\rm th}(t)$ from SNII and the gas binding energy $\Omega_{\rm g}(t)$ for models A1, A2, B, and C. The best fit MDFs of these models are realized at 0.03, 0.06, 0.31, and 0.28 Gyr, respectively

3.3.2. Model involving infall

The main weakness of model A1 is the poor fit of the left wing of the distribution (Fig. 5). The observed distribution is between A1 model and the infall model, which is much too wide (Fig. 3). This suggests that a model dominated by a more limited amount of infall at the beginning, and later on by the modified outflow model could give better fit. After all, a GC in formation is expected to benefit from infall; and outflow, even if it can partially overlap, may need several SNII explosions to become dominant. Since Cayrel (1986) suggested that star formation with a

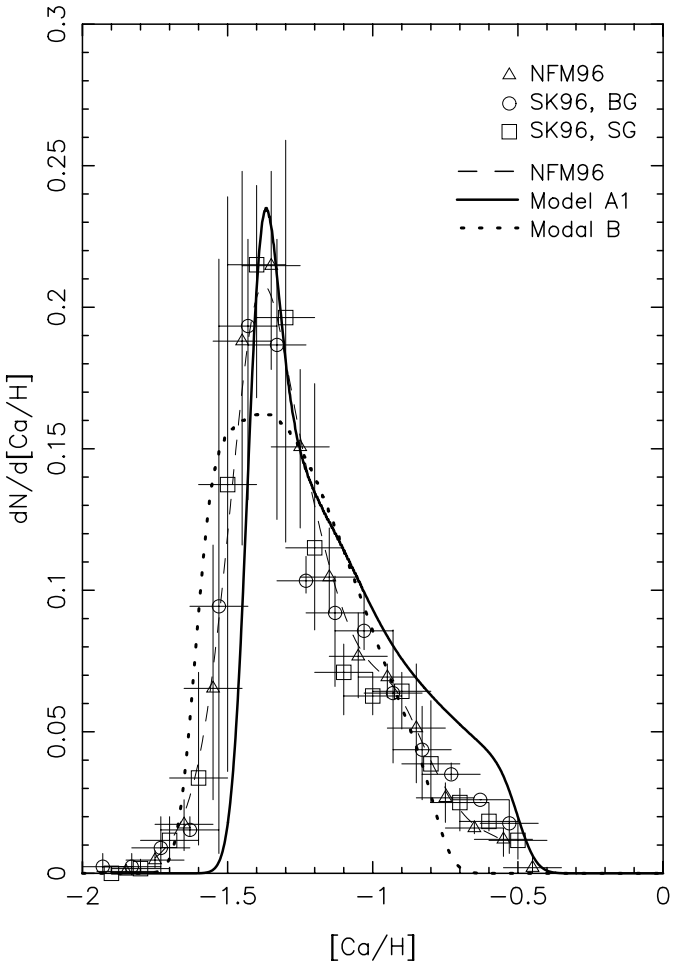

Fig. 5. Theoretical MDFs of models A1 (solid line) and B (dotted line). The dashed line gives the observed MDF of NFM96 sample. Symbols have the same meanings as those of Fig. 3

full mass spectrum occurs at a shock between the collapsing gas and the SNII-driven wind, we modify the previous model and construct an outflow model involving infall. Another possible cause of the poor fit of model A1 is our assumption that the mass range of newly formed stars changes abruptly before and after the first SNII explosion. We neglect the possibility of gradually changing lower mass cutoff in our model discussed below.

A chemo-dynamical simulation (Hensler & Burkert 1990) to study the ISM evolution in an open one-zone model showed that the gas outflow dominates most of the time while the inflow occurs during the phase of small internal pressure. Although the inflow discretely happens in their model, we assume continuous infall of gas for simplicity. The gas evolution is given as below:

$$\frac{dM_{\rm g}(t)}{dt} = -C(t) + E(t) + A(t) - B(t). \quad (26)$$

Other model prescriptions are the same as those of the previous outflow model with the bimodal IMF, therefore the primordial composition of collapsing gas is assumed. The number of combination of parameters becomes quite large in this case. Therefore, we first carry out a rough surveying calculation to find parameter area resulting in χ^2-values smaller than 40. The model grids are the following:

$$\begin{aligned}
&\tau_{\rm sf} = 0.001,\ \left[10^{-2.0+0.3i}\ (i=0,...,5)\right],\ 3\ \ {\rm Gyr},\\
&\tau_{\rm of} = 0.001,\ \left[10^{-2.0+0.3i}\ (i=0,...,5)\right],\ 3\ \ {\rm Gyr},\\
&\tau_{\rm in} = 0.001,\ \left[10^{-2.0+0.3i}\ (i=0,...,5)\right],\ 3\ \ {\rm Gyr},\\
&x = 1.0, 1.3, 1.5, 2.0, 2.3,\\
&T = 10^{-2.0+i\Delta T}\ (i=0,...,29)\ \ {\rm Gyr},\\
&[{\rm Ca/H}]_0 = -1.8, -1.6, -1.5, -1.4,
\end{aligned}$$

where $\Delta T = 7.25 \cdot 10^{-2}$ Gyr. Next, we simulate models by adopting the following parameters by considering results of the previous survey calculation:

$$\begin{aligned}
&\tau_{\rm sf} = 0.05, 0.07, 0.1, 0.15 && {\rm Gyr},\\
&\tau_{\rm of} = 0.15, 0.20, 0.25 && {\rm Gyr},\\
&\tau_{\rm in} = 0.02, 0.03, 0.04, 0.05, 0.06 && {\rm Gyr},\\
&x = 1.8, 1.9, 2.0, 2.1,\\
&T = 10.^{-2.0+i\Delta T}\ (i=0,...29) && {\rm Gyr},\\
&[{\rm Ca/H}]_0 = -\infty, -1.6, -1.5,
\end{aligned}$$

where $\Delta T = 7.25 \cdot 10^{-2}$ Gyr.

In Fig. 5, the dotted line shows the best-fit ($\chi^2 = 20.1$) model (model B), of which parameters and skewness are given in Table 1. Degrees of freedom of the χ^2 are seven. Evolution of $E_{\rm th}/\Omega_{\rm g}$ of model B is illustrated in Fig. 4. The epoch of $E_{\rm th}(t) = \Omega_{\rm g}(t)$ is realized at $T_{\rm w} = 0.40$ Gyr, which is well after the epoch ($T = 0.31$ Gyr) of establishing the best-fit MDF. Thus model B does not violate the $T < T_{\rm w}$ criterion. Both the left and right wings of the MDF of model B are fitted to the empirical MDF better than those of model A1. However, the peak of the MDF of model B is not sharp enough and more stars of [Ca/H] < -1.4 are formed than the observation. The latter discrepancy is similar to that of the previous infall model in Sect. 3.2. Again, this implies a smaller amount of infall. Thus we attempt to rectify the discrepancy by stopping the infall.

Theis et al. (1992) reported that the pressure of hot gas heated by the supernovae drives gas outflow and consequently the collapse of gas is stopped when ram pressure is neglected in their chemo-dynamical model for massive ($10^{11} - 10^{12} M_\odot$) spheroidal galaxies. Since they showed this as an extreme case to test influences of the ram pressure in the model, the situation might not reflect a realistic one. However, they suggested that dwarf galaxies might have a strong galactic mass loss even if the ram pressure is effective because of a shallower potential well. Since the mass (several $\times 10^6 M_\odot$) of ω Cen is smaller than those of dwarf galaxies ($10^7 - 10^9 M_\odot$), the gas inflow will be terminated by high internal pressure by supernovae heating. Although an epoch ($T_{\rm SN}$) of termination of the infall should be treated as a parameter, we simply set $T_{\rm SN}$ at an epoch of peak of SNII rate, since $T_{\rm SN}$ should be related to supernovae explosions. The following equation gives the gas evolution:

$$\frac{dM_{\rm g}(t)}{dt} = \begin{cases} -C(t) + E(t) + A(t) - B(t) & (t < T_{\rm SN}) \\ -C(t) + E(t) - B(t) & (t \geq T_{\rm SN}). \end{cases} \quad (27)$$

Other model prescriptions are the same as before. Similarly, we perform a rough surveying calculation, and then simulate

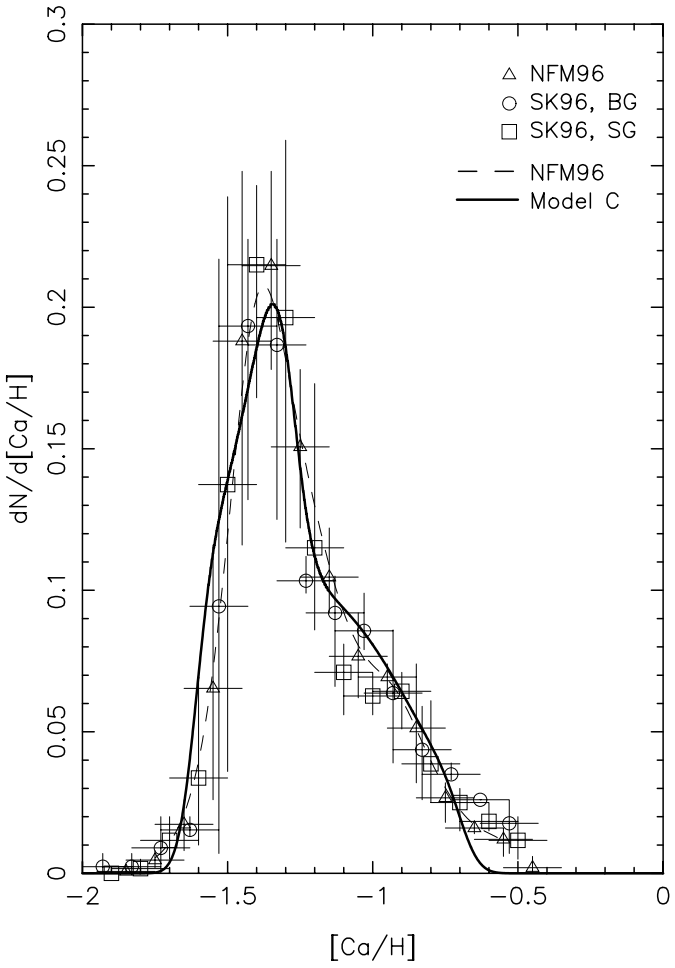

Fig. 6. Theoretical MDF of model C (solid line) and the observed MDF (dashed line) of NFM96 sample. Symbols have the same meanings as those of Fig. 3

models with the fine grids of parameters in the range of selected values. Model grids of the rough survey calculation are the same as those of the previous model. We choose the following model grids to find the best-fit model:

$$\begin{aligned}
&\tau_{\rm sf} = 0.05, 0.06, 0.07, 0.08, 0.09 \ \ {\rm Gyr},\\
&\tau_{\rm of} = 0.15, 0.20, 0.25 \qquad\quad {\rm Gyr},\\
&\tau_{\rm in} = 0.05, 0.06, 0.07, 0.08, 0.09 \ \ {\rm Gyr},\\
&x = 1.9, 2.0, 2.1,\\
&T = 10^{-2.0+i\Delta T}\ (i = 0, ..., 29) \ \ {\rm Gyr},
\end{aligned}$$

$$[{\rm Ca/H}]_0 = -1.6, -1.5, -1.4,$$

where $\Delta T = 7.25 \cdot 10^{-2}$ Gyr.

In Fig. 6, the solid line shows the best-fit model (model C) with $\chi^2 = 4.5$, the degrees of freedom of the χ^2-test become eight. Model C fits to the observed MDF very well, as a quite good χ^2-value shows. The parameters of model C are summarised in Table 1 together with the χ^2-value and the skewness. The epoch of the termination of the inflow, i.e., the peak epoch of SNII rate, is realized at $T_{\rm SN} = 0.08$ Gyr. Model C is characterised by small $\tau_{\rm in}$ and $\tau_{\rm sf}$ ($\tau_{\rm in} = \tau_{\rm sf} = 0.07$ Gyr), relatively large $\tau_{\rm of}$ ($= 0.2\tilde{\rm G}$yr) and a steep IMF ($x = 1.9$). The parameters obtained are roughly the same as those of model B. The evolution of $E_{\rm th}/\Omega_{\rm g}$ is illustrated in Fig. 4. The epoch of $E_{\rm th}(t) = \Omega_{\rm g}(t)$ is $T_{\rm w} = 0.31$ Gyr, while the resulting duration of star formation is $T = 0.28$ Gyr. These satisfy the criterion discussed previously. We also note that T is much shorter than a typical lifetime ($\sim 1 - 2$ Gyr) of SNIa and is consistent with the argument in Sect. 2. Thus, model C gives far better fit than any other models studied in this paper.

4. Discussion

4.1. Abundance gradient

In Fig. 7a, we plot an abundance distribution on the projected surface of ω Cen, where the coordinate corresponds to that of the photographic plate of the ROA catalogue (Woolley 1966) and the abundances are taken from NFM96. Metal-poor populations are shown by open squares ([Ca/H]< -1.5) and triangles ($-1.5 \leq [{\rm Ca/H}] < -1.25$), while metal-rich populations are given by filled diamonds ($-1.25 \leq [{\rm Ca/H}] < -1.0$) and triangles ($-1.0 \leq$ [Ca/H]). There is no obvious difference between distributions of metal-poor and metal-rich stars. Fig. 7b represents a radial distribution of [Ca/H]. The abundance and the positional data are taken from NFM96 and Mayor et al. (1997), respectively. Omega Cen is a flattened GC and the ellipticity changes as a function of distance from the centre. Although we could have plotted an ellipsoidal radius, we do not attempt this in order to avoid confusion by projection effects. In this diagram, there is no clear abundance gradient. However, we notice that metal-rich ([Ca/H]> -0.5) stars do not exist at the outer part of ω Cen and that most of stars are located near [Ca/H] $\simeq -1.4$ independent of the radius. To see the abundance distribution at a particular radius, we divide the samples into four bins and calculate the corresponding MDFs. We limit the MDFs for [Ca/H]< -0.5. In Fig. 7c, we illustrate the MDF in each bin, which is weighted by the number of stars contained in the corresponding bin. The peaks appear almost at the same [Ca/H] except for the outermost bin where MDF has an irregular shape due to a small number of stars. There are second peaks for the MDFs of the innermost two bins at [Ca/H]$\simeq -0.9$. We do not pay attention to these peaks because of the concern about the sampling effects. We find that contribution from metal-rich stars declines from the inner bin to the outer.

Now we consider why metal-rich stars decrease toward the outer region. As we have argued before, the gas outflow must occur during star formation of ω Cen. The potential well of the outer region should be shallower than that of the inner and the gas in the outer region is more easily expelled. Hence duration of star formation in the outer is expected to be shorter than in the inner, resulting in less progress of chemical evolution in the outer region.

Gas outflow which starts from the outer part of a system will also occur in elliptical galaxies, since GCs and ellipticals are suggested as one parameter family (Yoshii & Arimoto 1987). Spectroscopic measurements of Mg_2 index (e.g., Carollo

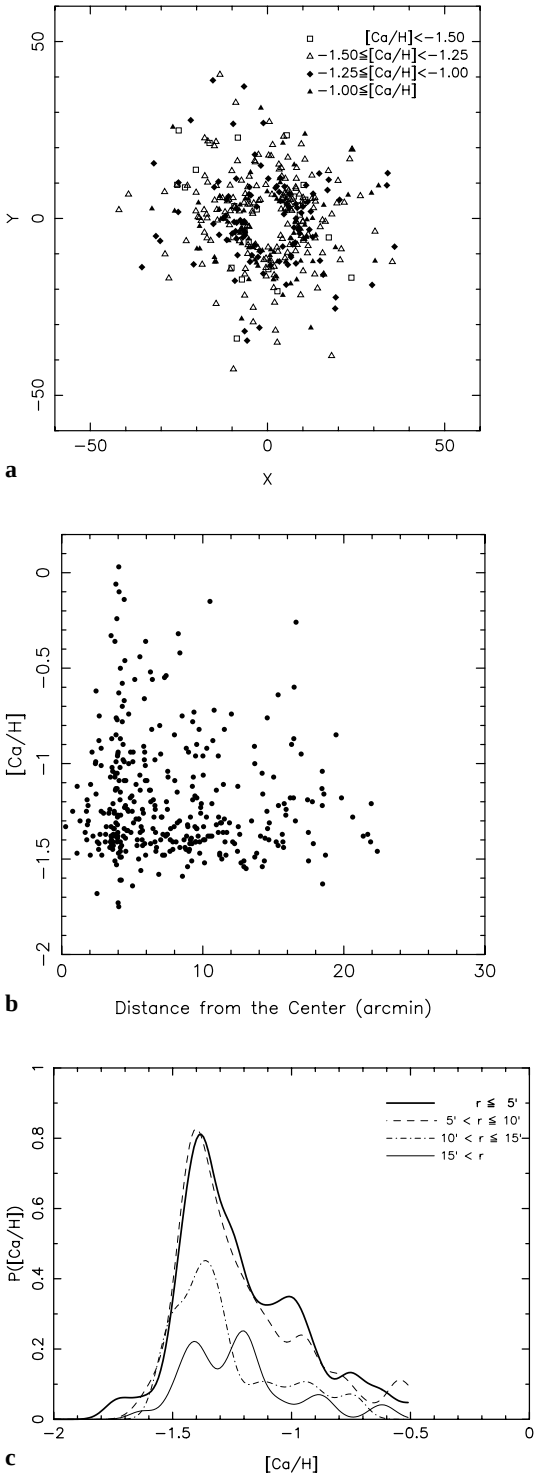

Fig. 7a–c. a A map of calcium abundance. The coordinate corresponds to that of the ROA catalogue (Woolley 1966). The abundance data is taken from NFM96. Each symbol represents different abundance of stars, which is indicated in the panel. **b** Dependence of [Ca/H] on radial distance. The abundance data and the distance are taken from NFM96 and Mayor et al. (1997), respectively. **c** A comparison of MDFs at different distance from the centre. They are weighted by a number of stars in each bin. Lines are labelled inside the panel with the distance range of the bin

& Danziger 1994) of elliptical galaxies show that the colour gradients come from metallicity changes. Franx & Illingworth (1990) found that colour gradients, or metallicity gradients in elliptical galaxies are related with local escape velocity and concluded that the origin of the gradients is the gas outflow because alternative models such as gas inflow and mergers should not result in the correlation between the local escape velocity and the metallicity. Martinelli et al. (1998) investigated whether the metallicity gradients in elliptical galaxies can be explained by assuming an earlier epoch of galactic wind at outer region where the potential well is shallower than the inner region. If ellipticals have experienced the gas outflow, their MDFs are expected to have a metal-rich tail.

4.2. Enrichment in GCs

The self-enrichment can well explain the metallicity dispersion of ω Cen. Based on their numerical simulation for SNRs in a cloud, Morgan & Lake (1989) inferred that ω Cen is massive enough to survive against energy injection from generations of SNII. A deep gravitational potential could be a reason why only ω Cen clearly shows evidence of gas recycling. In proto-clouds of other smaller GCs, the gas would be expelled immediately after the first SNII explosion because of their shallower potential well. As we have already discussed, formation of low mass stars should follow that of high mass stars. In less massive systems, gas recycling and star formation with a full spectrum of stellar mass will be terminated much earlier than in ω Cen. If this is the case, long-lived stars in every GC should be formed in already enriched gas and their composition will be almost the same. This implication is consistent with observed cutoff of lower metallicity of the Galactic GC system and homogeneous composition for each Galactic GC (e.g. Harris 1991). The lower metallicity cutoff ([Fe/H]$\lesssim -2$) seems nearly the same for globular cluster systems (GCSs) in extragalactic systems as well. For example, Fig. 8 of Harris (1991) shows that the cutoff is located at [Fe/H]$\lesssim -2$, which is common for a giant elliptical NGC 5128 and dwarf ellipticals. The *Hubble Space Telescope* observation (Kundu & Whitmore 1998) for the GCS of S0 galaxy NGC 3115 also shows such a lower metallicity cutoff, which is estimated [Fe/H]$\lesssim -2$ by using their conversion equation from colour to the iron abundance. If long-lived stars in the GCs were born in enriched gas, these phenomena can be naturally explained. Hence, the idea of self-enrichment in GCs presented by Cayrel (1986) is favourable. Needless to say, if the metallicity of proto-cloud is already higher than [Fe/H]$\simeq -2$, owing to chemical enrichment by halo field stars, the abundance increase via self-enrichment is negligible and all stars in GCs should have the same abundances as their mother clouds.

There is a discrepancy in the time span of star formation between the best-fit model (model C) and the work presented by Hughes & Wallerstein (1998). Based on accurate Strömgren photometry of stars at the main-sequence of ω Cen, they plotted a colour-magnitude diagram with isochrones and derived the age difference (~ 4 Gyr). On the other hand, model C has a much shorter span of 0.28 Gyr. Since they used the so-called

isochrone-fitting method to estimate a difference in age, the resulting age span of course depends on stellar evolutionary tracks adopted. For example, adopting a similar method, Noble et al. (1991) concluded that a colour distribution in the main sequence of ω Cen is consistent with the metallicity distribution in more evolved stars such as subgiants, giants, and horizontal branch stars. In addition to this, such a long time span of star formation over a lifetime of SNIa ($1 - 2$ Gyr) is inconsistent with the empirical abundance patterns (Norris & Da Costa 1995) which are α-enhanced, even in the metal-rich tail. Thus the result of model C can explain the chemical properties observed in ω Cen better than that of Hughes & Wallerstein (1998).

5. Conclusion

We have investigated the origin of the metallicity dispersion observed in ω Cen and explored whether the self-enrichment scenario can explain the dispersion. Models are confronted with the observed MDFs by NFM96 and SK96. The empirical MDF is characterised by a rapid increase from lower metallicity to the peak metallicity and a gradual decrease towards higher metallicity, i.e. a metal-rich tail. We construct five models. The first three are the closed-box, the outflow, and the infall models, which all result in inconsistent MDFs with the observation. Next, the outflow models with the bimodal IMF are constructed, where long-lived stars are assumed to form after the first SNII explosions. This model gives a better fit to the empirical MDFs than any other first three models, but the fit is not yet perfect. Finally, we modified the previous model of the bimodal IMF and obtained the best-fit model. In this model we assume a gas infall at the beginning and the bimodal IMF. A view of chemical enrichment obtained by the best-fit model is as follows: a rapid gas infall occurs at the beginning and only massive stars form. After the first SNII explosions, star formation of a full spectrum range in mass occurs and chemical enrichment progresses. The gas infall is terminated due to SNII heating, which leads to a gas outflow. Because of gas consumption and the outflow, star formation is ceased. The resulting duration of star formation is 0.28 Gyr and is shorter than the typical lifetime ($\sim 1-2$ Gyr) of SNIa. This is consistent with the observation which showed super-solar ratios of [α/Fe] of stars in ω Cen (Norris & Da Costa 1995). Thus we conclude that the self-enrichment is the origin of the abundance dispersions in ω Cen.

Our study shows that the view of the formation and evolution of ω Cen agrees with that of GCs predicted by Cayrel (1986): the gas accretes to the centre of a proto-cloud, where only massive stars form at first. Subsequently star formation with a full mass spectrum occurs at a shocked region between the collapsing gas and the wind driven by supernovae. The gas is expelled due to a strong energy injection by SNII. This leads to termination of star formation. This scenario can naturally explain the universal low-metallicity cutoff of GCSs observed at [Fe/H]$\lesssim -2$ in elliptical galaxies. All GCs should survive at least one SNII, which enriches the surrounding gas. Long-lived stars formed after the SNII explosion, and hence always contained metals. Therefore, ω Cen may be an analogue of small spheroidal galaxies and provides the simplest and best opportunity currently available to investigate how such a system chemically enriches itself. We expect that similar studies of the MDFs will reveal chemical enrichment and star formation histories of dwarf galaxies in the Local Group.

Acknowledgements. The authors are both grateful and indebted to the referee, R. Cayrel, for his helpful remarks and suggestions on the early version of their models and the paper. C.I. thanks T. Kodama for fruitful discussion and the Japan Society for Promotion of Science for a financial support. This work was financially supported in part by a Grant-in-Aid for Scientific Research (No. 11640230) by the Japanese Ministry of Education, Culture, Sports and Science.

References

Arimoto N., Yoshii Y., 1987, A&A 173, 23
Bhatt H.C., 1988, MNRAS 233, 867
Butler D., Dickens R.J., Epps E., 1978, ApJ 225, 148
Cannon R.D., Stobie R.S., 1973, MNRAS 162, 207
Carollo C.M., Danziger I.J., 1994, MNRAS 270, 523
Cayrel R., 1986, A&A 168, 81
Cox D.P., 1972, ApJ 178, 159
Cudworth W.M., 1976, AJ 81, 519
Dauphole B., Geffert M., Colin J., et al., 1996, A&A 313, 119
Dickens R.J., Woolley R.v.d.R., 1967, R. Obs. Bull. No. 128
Edvardsson B., Andersen J., Gustafsson B., et al., 1993, A&A 275, 101
Franx M., Illingworth G., 1990, ApJ 359, L41
Freeman K.C., Norris J., 1981, ARA&A 19, 319
Freeman K.C., Rodgers A.W., 1975, ApJ 201, L71
Harris W., 1991, ARA&A 29, 543
Harris W.E., Racine R., 1979, ARA&A 17, 241
Hensler G., Burkert A., 1990, Ap&SS 171, 149
Hills J.G., 1980, AJ 225, 986
Hughes J.D., Wallerstein G., 1998, A&AS 193, 6809H
Icke V., Alcaíno G., 1988, A&A 204, 115
Ikeuchi S., 1977, Prog. Theor. Phys. 58, 1742
Ikuta C., Arimoto N., 1999, PASJ 51, 459
Kraft R.P., 1979, ARA&A 17, 309
Kraft R.P., 1994, PASP 106, 553
Kundu A., Whitmore B.C., 1998, AJ 116, 2841
Laird J.B., Rupen M.P., Carney B.W., Latham D.W., 1988, AJ 96, 1908
Lee S., Schramm D.N., Mathews G., 1995, ApJ 449, 616
Lehnert W.D., Bell R.A., Cohen J.G., 1991, ApJ 367, 514
Martinelli A., Matteucci F., Colafrancesco S., 1998, MNRAS 298, 42
Makino J., Akiyama K., Sugimoto D., 1991 Ap&SS 185, 63
Meylan G., 1987, A&A 184, 144
Meylan G., Mayor M., 1986, A&A 166, 122
Meylan G., Mayor M., Duquennoy A., Dubath P., 1995, A&A 303, 761
Mayor M., Meylan G., Udry S., et al., 1997, AJ 114, 1087
Morgan S., Lake G., 1989, ApJ 339, 171
Noble R.G., Dickens R.J., Buttress J., Griffiths W.K., Penny A.J., 1991, MNRAS 250, 314
Nomoto K., Thielemann F.-K., Yokoi K., 1984, ApJ 286, 644
Norris J.E., Da Costa G.S., 1995, ApJ 447, 680
Norris J.E., Freeman K.C., Mighell K.J., 1996, ApJ 462, 241, (NFM96)
Norris J.E., Freeman K.C., Mayor M., Seitzer P., 1997, ApJ 487, L187
Saito M., 1979, PASJ 31, 181
Searle L., 1977, In: Tinsley B.M., Larson R.B. (eds.) The Evolution of Galaxies and Stellar Populations. Yale Univ. Obs., New Haven, p. 219

Searle L., Zinn R., 1978, ApJ 225, 357
Smith G.H., 1987, PASP 99, 67
Suntzeff N.B., Kraft R.P., 1996, AJ 111, 1913, (SK96)
Theis Ch., Burkert A., Hensler G., 1992, A&A 265, 465
Thielemann F.-I., Nomoto K., Hashimoto M., 1996, ApJ 460, 408
Tinsley B.M., 1980, Fund. Cosm. Phys. 5, 287
Trager S.C., King I.R., Djorgovski S., 1995, AJ 109, 218
Tsujimoto T., Nomoto K., Yoshii Y., et al., 1995, MNRAS 277, 945
Woolley R.v.d.R., 1966, R. Greenwich Obs. Ann., 2
Yoshii Y., Arimoto N., 1987, A&A 188, 13